

A preliminary study to understand the transport process for the eggs and larvae of Japanese Pacific walleye pollock *Theragra chalcogramma* using particle-tracking experiments based on a high-resolution ocean model

Hiroshi Kuroda · Daisuke Takahashi ·
Humio Mitsudera · Tomonori Azumaya ·
Takashi Setou

Received: 31 March 2013 / Accepted: 1 September 2013 / Published online: 14 March 2014
© The Japanese Society of Fisheries Science 2014

Abstract We developed a realistic $1/50^\circ$ high-resolution ocean model capable of resolving submesoscale variability, and performed particle-tracking experiments based on this ocean model to identify elements that significantly affect the transport of the eggs and larvae of the Japanese Pacific walleye pollock *Theragra chalcogramma* into Funka Bay. The high-resolution model reproduced representative features of the oceanographic conditions of the main spawning area and season. A comparison of particle-tracking experiments performed under the passive transport condition based on high-resolution ($1/50^\circ$) and low-resolution ($1/10^\circ$) ocean models showed that high-resolution modeling is essential in order to realistically simulate

the transport process. In this regard, however, the vertical motion of particles cannot be explained by the passive transport condition, as it leads to unrealistically deep sinking of particles in the simulation. Turning our attention to feasible non-passive transport conditions, we then incorporated the buoyancy motion of particles and conducted additional experiments that mainly differed in the particle density adopted. We clarified that buoyancy is an important factor in the retention of particles near the sea surface, and that the ratio of the particles that remain in Funka Bay to the number of particles released is sensitive to the vertical motions/positions of the particles, implying that it is necessary to model this vertical motion more accurately by incorporating more realistic biological processes or a statistical distribution into the particle-tracking model.

This article is sponsored by the Fisheries Research Agency, Yokohama, Japan.

Electronic supplementary material The online version of this article (doi:10.1007/s12562-014-0717-y) contains supplementary material, which is available to authorized users.

H. Kuroda (✉) · T. Azumaya
Hokkaido National Fisheries Research Institute, 116 Katsurakoi,
Kushiro, Hokkaido 085-0802, Japan
e-mail: kurocan@affrc.go.jp

H. Kuroda · T. Setou
National Research Institute of Fisheries Science,
2-12-4 Fukuura, Kanazawa, Yokohama,
Kanagawa 236-8648, Japan

D. Takahashi
Graduate School of Agricultural Science, Tohoku University,
1-1 Amamiya, Tsutsumidori, Aoba, Sendai, Miyagi 981-8555,
Japan

H. Mitsudera
Institute of Low Temperature Science, Hokkaido University,
Nishi-8, Kita-19, Sapporo, Hokkaido 060-0819, Japan

Keywords Eggs and larvae · Funka Bay ·
Particle-tracking experiment · ROMS ·
Submesoscale variability · Walleye pollock

Introduction

The Japanese Pacific walleye pollock *Theragra chalcogramma* is distributed across the northwestern Pacific region off the coast of Hokkaido and Tohoku [1], and is one of the most important target species for Japanese commercial fisheries. In recent years, the stock of this population has tended to be sustained by the occasional occurrence of strong year-classes [2]; in other words, after the occurrence of a strong year-class, most of the catch—as well as the population—comes from this year-class, and this situation lasts for several years. Oceanographic and food conditions can determine year-class strength during

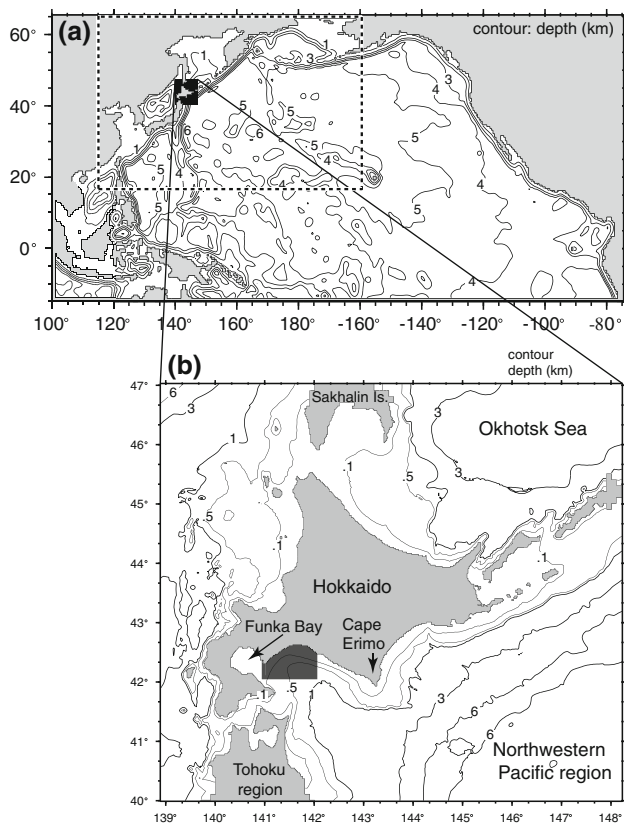


Fig. 1 **a** Model domain of the $1/2^\circ$ model. The region in the *dashed square* corresponds to the $1/10^\circ$ model domain. **b** The $1/50^\circ$ model domain. In the PT experiments, the particles were initially arranged inside the *dark gray area*

the early life stages of the fish [3], but the process of and mechanism for generating strong year-classes is not yet understood in detail.

In the study reported in the present paper, we focused on transport processes of walleye pollock during its early life stages, such as its eggs and larvae, which are considered to be key influences on the stocks and recruitment of this fish. For instance, it has been reported that the transport process is a critical factor in the recruitment dynamics of walleye pollock in Shelikof Strait, Gulf of Alaska [4], the occurrence of strong or weak year-classes (through the adult–child encounter frequency, i.e., cannibalism) in the Bering Sea [5], and the genetic stock structure in the region from the Bering Sea to the Gulf of Alaska [6]. The transport process around the spawning ground has also been suggested to be an important factor for the specific case of Japanese Pacific walleye pollock, as follows.

Japanese Pacific walleye pollock spawn mainly in January and February on the continental shelf around Funka Bay (Fig. 1) [7, 8]. Some of the resulting eggs and larvae

are transported southward to the Tohoku region, and some are transported into Funka Bay and remain within this bay [9]. During May to June, the grown juveniles leave Funka Bay and move eastward along the Hokkaido coast to the nursery ground east of Cape Erimo [10]. Thus, it appears that one of the conditions favoring recruitment is the transport of eggs and larvae into the bay and their residence there until spring [11].

During the main spawning season (January–February), seasonal currents near the sea surface around Funka Bay are characterized by two flows: the Coastal Oyashio (CO) and the wind-driven current [12]. The CO is a boundary current that is trapped against the Pacific shelf-slope region and transports very cold and low-salinity water, referred to as CO water, from the Okhotsk Sea to the vicinity of Funka Bay [13]. During this season, the northwesterly wind is dominant around Hokkaido, and this drives southeastward flows at the sea surface near the coast. As a result, the CO and wind-driven currents are superposed on the shelf-slope region near Funka Bay.

Shimizu and Isoda [14] examined the individual effects of the CO and wind-driven currents on the transport of walleye pollock eggs using a particle-tracking (PT) model based on an idealized two-dimensional barotropic ocean model. Recently, Sakamoto et al. [15] pointed out that a high-resolution three-dimensional ocean model with a grid size of less than a few kilometers is required to appropriately reproduce the CO. This suggests that such high-resolution three-dimensional modeling is also required to investigate the transport process of the eggs and larvae of Japanese Pacific walleye pollock.

The present study was conducted as preliminary work in the development of an individual-based model (IBM) of Japanese Pacific walleye pollock that can systematically integrate oceanographic and biological studies into an interdisciplinary framework. The first aim of this study was to develop a high-resolution three-dimensional ocean model which can reproduce realistic oceanographic conditions around Funka Bay under climatological forcings. The second aim was to identify the elements that significantly affect the transport of walleye pollock eggs and larvae into Funka Bay using PT experiments. The significance of utilizing high-resolution ocean modeling in the PT experiments was investigated by comparing the results obtained with those produced by low-resolution modeling under the passive transport condition. It was found that the passive transport condition led to the unrealistic sinking of particles in the simulation. Therefore, turning our attention to feasible non-passive transport conditions, we incorporated particle buoyancy effects and studied the significance of the vertical motions/positions of the particles.

Materials and methods

High-resolution submesoscale ocean model

We developed a triply nested high-resolution model using the Regional Ocean Modeling System (ROMS) [16, 17]. Three models with different resolutions ($1/2^\circ$, $1/10^\circ$, and $1/50^\circ$) were connected by one-way nesting (Fig. 1) [18, 19]. All of the models were forced by climatological fluxes at the sea surface and the lateral boundary. The design details for the $1/2^\circ$ and $1/10^\circ$ models are described in Kuroda et al. [20], and those for the $1/50^\circ$ model are explained below.

The $1/50^\circ$ model domain covered all of the coastal regions around Hokkaido (Fig. 1). The vertical resolution was 21 levels. For tracer and momentum advection, third-order upstream-biased and fourth-order centered schemes were applied for the horizontal and vertical directions, respectively. A bi-harmonic operator was adapted for horizontal mixing along the S-surface (Smagorinsky constant = 0.08).

The $1/50^\circ$ model was driven by fluxes at the sea surface and at the lateral boundaries. Heat, salinity, and momentum fluxes at the sea surface were computed using meteorological elements derived from normal-year forcing (CORENYF), such as wind velocity, air temperature, sea surface pressure, relative humidity, precipitation, and shortwave and downward longwave radiation [21]. The freshwater flux at the sea surface was weakly corrected based on the monthly mean climatology (WOA2001) with a timescale of 30 days. Meanwhile, the freshwater flux from the land (such as that arising from river discharges) was neglected because the primary target of our simulation was the main spawning season—winter, which is associated with only small river discharges.

A 20-year simulation was implemented using three models. The $1/50^\circ$ model was integrated for the final 5 years, from the 16th to the 20th year. The initial value was obtained through bi-linear interpolation from the output of the $1/10^\circ$ model on 1 January in the 16th year. The lateral boundary value was extracted from the 3.8-day mean output of the $1/10^\circ$ model. We analyzed the simulation of the final 4-years. In the next section, the reference time for model integration, the 16th to the 20th year, is changed and referred to as the 1st to the 5th year.

Particle tracking model

Using the simulated oceanographic conditions, we conducted particle-tracking experiments to understand the transport process for the walleye pollock eggs and larvae into Funka Bay. The PT model was based on LTRANS (ver. 1) (Schlag et al., *Larval TRANSPORT Lagrangian Model User's Guide*, 2008), which is configured for ROMS

output, but the source codes were modified to suit our model's configuration and purpose.

Initially, particles were set to a depth of 10 m in the gray region of Fig. 1b, which is associated with the main spawning ground [22–24]. The initial position at a depth of 10 m was determined simply on the basis of the position of the mode of the measured vertical egg distribution (see Fig. 10) [25]. In fact, eggs are probably spawned at depths of about 100 m [26] and then transported upward, but these processes are omitted from the PT experiments for the sake of simplification. The initial spatial interval between adjacent particles was 0.005° (=0.42–0.56 km). About 20,000 particles were tracked for 2 months from 1 February to 31 March using the methods explained in the subsequent paragraphs. The 2 months correspond to the egg (~ 10 – 20 days [27]), pre-larval (~ 30 – 45 days [28]), and post-larval (~ 30 – 35 days [28]) stages. It was assumed throughout this study that the ability of the larvae to swim can be neglected.

Passive and non-passive transport conditions were employed for the PT experiments. The movements of particles under the passive condition were obtained as follows. The particle's position (x_{n+1} , y_{n+1} , z_{n+1}) at a time step of $n + 1$ is determined by its previous position at a time step of n and the three-dimensional model velocity (u_{model} , v_{model} , w_{model}):

$$\begin{cases} x_{n+1} = x_n + u_{\text{model}}\delta t \\ y_{n+1} = y_n + v_{\text{model}}\delta t, \\ z_{n+1} = z_n + w_{\text{model}}\delta t \end{cases} \quad (1)$$

where δt is the integration time step (=487 s). Turbulent diffusion is neglected under the passive transport condition. Two kinds of PT experiments (case H0 and case L0) were performed using the velocities from the $1/50^\circ$ and $1/10^\circ$ models (driven by the same sea surface forcings), and these were compared with each other to clarify the impacts of high-resolution modeling on the particle transport process.

PT experiments were also carried out under the non-passive transport condition. This was done because, under the passive condition, some of the particles were transported downward more than 100 m to the deep subsurface, and eggs and larvae have not been observed this deep. We therefore incorporated a feasible non-passive condition by including the effect of the density/buoyancy of particles on the vertical motion; laboratory experiments suggest that this effect is significant [27, 29]. In addition, the turbulent diffusion was added to the vertical motion of particles under the non-passive transport condition because a large vertical diffusive coefficient is predicted within the winter mixed layer in the $1/50^\circ$ model.

The governing equation (1) was modified by adding the terminal buoyancy velocity (as derived from Stokes' law) and the corrected random walk [30] to the vertical motions of the particles, as follows:

$$z_{n+1} = z_n + (w_{\text{model}} + w_{\text{buoyancy}})\delta t + K'_V \delta t + R\sqrt{2r^{-1}K_V\delta t}, \quad (2)$$

where K_V is the vertical eddy diffusive coefficient estimated by the KPP scheme in the 1/50° model, R is a random number with a mean of zero and a standard deviation of r , and K'_V is the vertical gradient of K_V .

The upward terminal buoyancy velocity (w_{buoyancy}) was determined via

$$w_{\text{buoyancy}} = \frac{1}{18}gd^2 \frac{\rho_{\text{water}} - \rho_{\text{particle}}}{\rho_{\text{water}}} \nu^{-1}, \quad (3)$$

where g is the acceleration at the Earth's surface due to gravity (9.8 m/s^2), d is the particle's diameter ($1.5 \times 10^{-3} \text{ m}$), ρ_{particle} is the particle's density, ρ_{water} is the density of the water in the simulation, and ν is the kinematic viscosity ($1.5 \times 10^{-6} \text{ m}^2/\text{s}$ for water at $5 \text{ }^\circ\text{C}$).

Five PT experiments were conducted with different particle densities: 1023 kg/m^3 (case H1), 1024 kg/m^3 (case H2), 1025 kg/m^3 (case H3), 1026 kg/m^3 (case H4), and 1026.5 kg/m^3 (case H5). The particle densities in cases H1–H3 were within the range of egg densities ($1020\text{--}1025 \text{ kg/m}^3$) measured in laboratory experiments [27]. The particle density in case H4 (H5) was slightly smaller (greater) than the ambient water density in the winter mixed layer around Funka Bay.

It should be noted that the particle density and diameter were not varied in the PT experiments. However, in reality, these parameters can vary together with the growth [27, 29]. This idealization was used because there were significant uncertainties in several biological parameters and behaviors. For example, there have been no reports of the changes in larval density over time, the changes in egg and larval densities as functions of seawater pressure, or the variation in larval shape over time, which is required to derive an accurate buoyancy velocity for a nonspherical larva (rather than Stokes' law, which is limited to a spherical body). In addition, Sakurai and Yamamoto (pers. comm., 2013) recently proposed that the vertical distribution of the larvae depends on the temperature profile in the water column, thus suggesting active vertical migration of the larvae.

Hence, in this study, the particle density can be regarded as a turning parameter to control the vertical positions of particles. In our experiments, the particle diameter was fixed to the egg diameter ($1.5 \times 10^{-3} \text{ m}$), which was equivalent to the minimum size of a larva. That is, since the buoyancy

velocity is proportional to the square of the diameter (Eq. 3), the buoyancy velocity given in our experiment corresponded to the minimum value during the larval stage.

Results

Reproducibility of the high-resolution model

The simulated 4-year mean salinity and current at the sea surface in February (i.e., during the main spawning season) are plotted and shown schematically in Fig. 2. During this month, low-salinity (high-salinity) water corresponds to cold (warm) water. The very-low-salinity water, referred to as the East Sakhalin Current water, is distributed in the

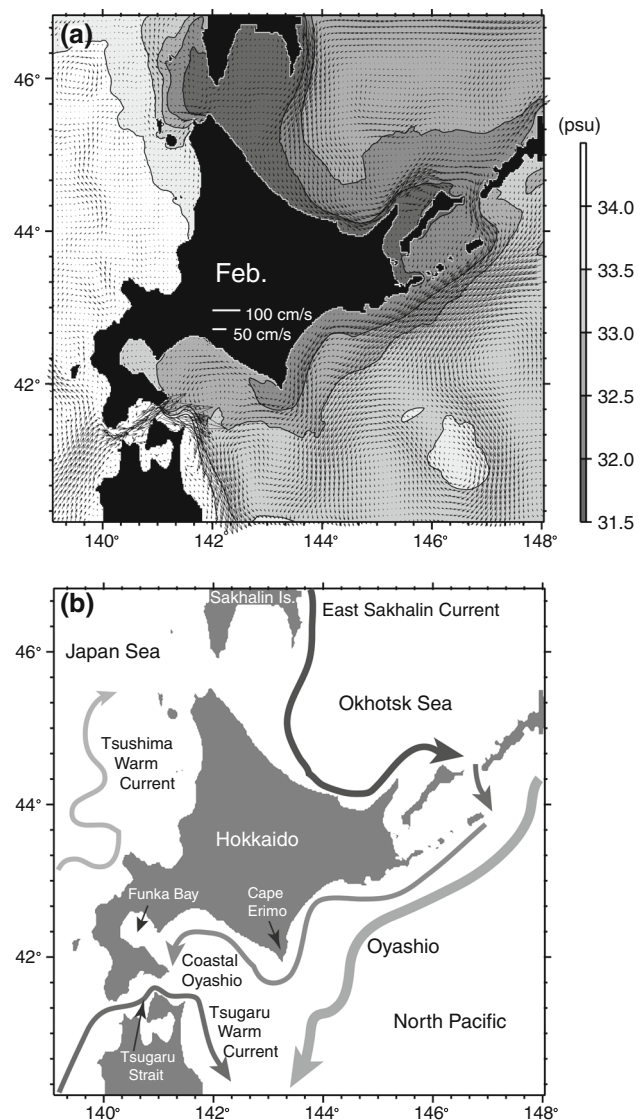


Fig. 2 a Four-year mean salinities and currents at the sea surface in February. b Schematic view

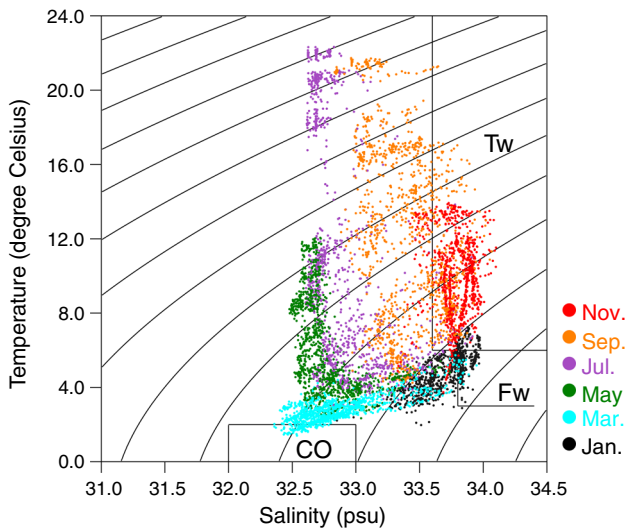


Fig. 3 Scatter diagram of bi-monthly temperatures and salinities at depths of 0, 20, 40, 60, and 80 m at 20 fixed positions in Funka Bay. CO, Tw, and Fw are typical water systems in Funka Bay [44]

Okhotsk Sea [31]. This water is transported southward along the eastern coast of Sakhalin Island by the East Sakhalin Current, which intensifies greatly in late autumn and winter [32–36]. Meanwhile, the Soya Warm Current that flows along the Hokkaido coast in the Okhotsk Sea, as reported in observational studies, cannot be seen [37]. Some of the water in the East Sakhalin Current flows out from the Okhotsk Sea into the North Pacific, as it is modified into CO water because it mixes with ambient water [15, 38, 39]. The CO water is transported along the southern coast of Hokkaido toward Funka Bay by the CO [12, 15, 40]. The CO is independent of the Oyashio flowing southwestward on the offshore slope [41]. The CO comes into contact with the Tsugaru Warm Current at the eastern mouth of the Tsugaru Strait [42]; the outflow from this exhibits the coastal mode during this month [43]. Consequently, these consistencies suggest that our model successfully reproduces the representative oceanographic conditions around Hokkaido during the main spawning season of the walleye pollock.

The simulated temperatures and salinities at 20 fixed horizontal positions in Funka Bay are plotted in the TS diagram in Fig. 3. Typical water-mass exchanges and modifications that occur from autumn to spring, which are representative features of Funka Bay during the spawning season of the walleye pollock [44], were successfully simulated for the first time using the three-dimensional high-resolution model. In November, the Tsugaru Warm Current water (“Tw”) occupies the whole bay. In January, the Tw is modified into dense Funka Bay water in winter (“Fw”) due to energetic sea surface cooling. The density of the simulated Fw is in the range 26.6–26.9 σ_T , which is

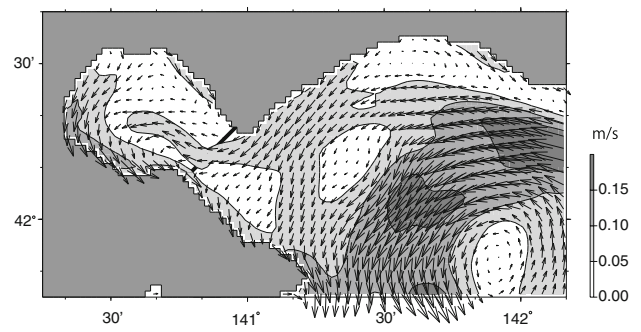


Fig. 4 Four-year mean current at the sea surface around Funka Bay. Background shading indicates current speed

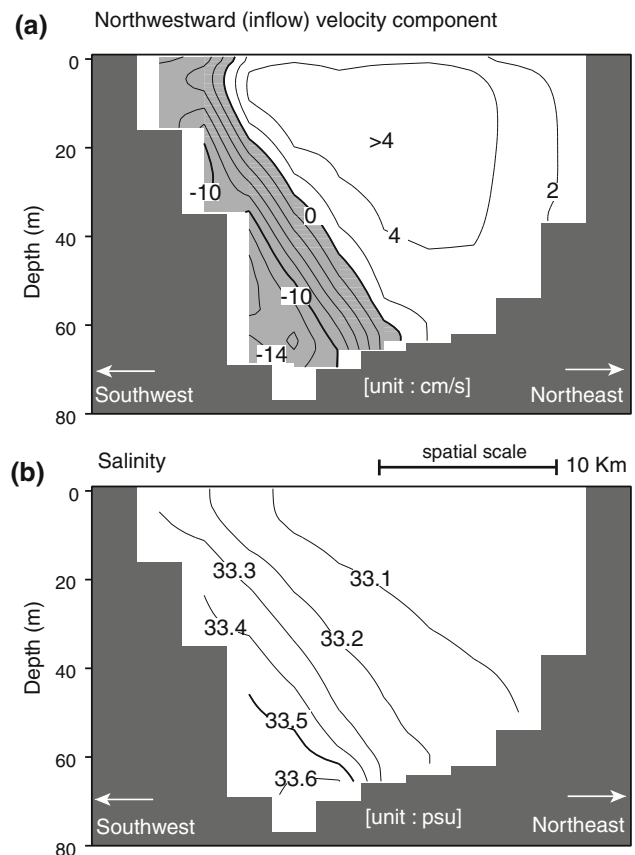


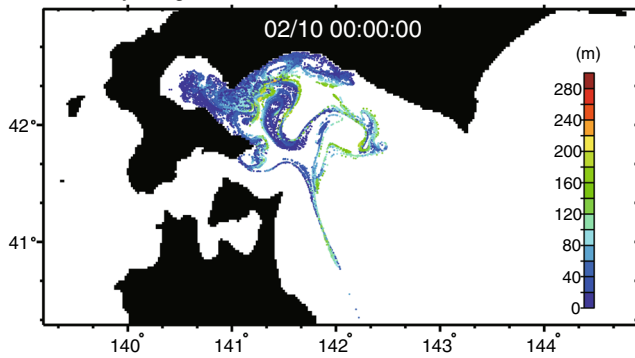
Fig. 5 a Four-year mean northwestward velocity components in February along the transect indicated by the *thick line* in Fig. 4. **b** Same as a, but for the salinity

consistent with that of the observed Fw [45]. Moreover, most of the Fw disappears in March, since it is rapidly replaced by the Coastal Oyashio water (“CO”) in February.

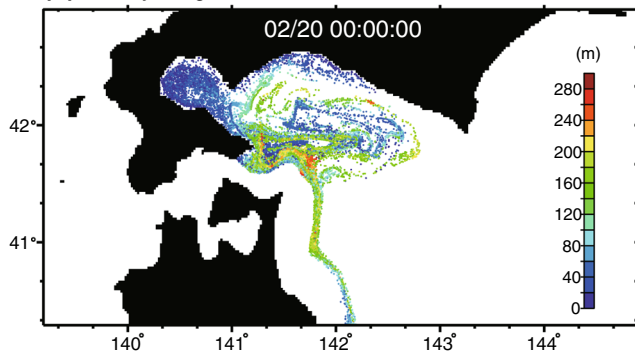
To examine the intrusion pathway of the CO water into Funka Bay, we predicted the average velocity map at the sea surface for February (Fig. 4). The flow pattern is

Case H0

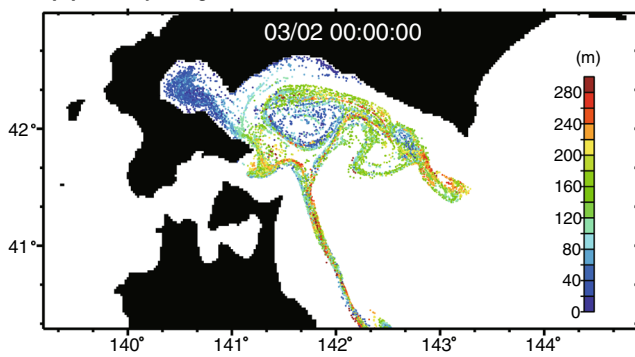
(a) 10-day Integration



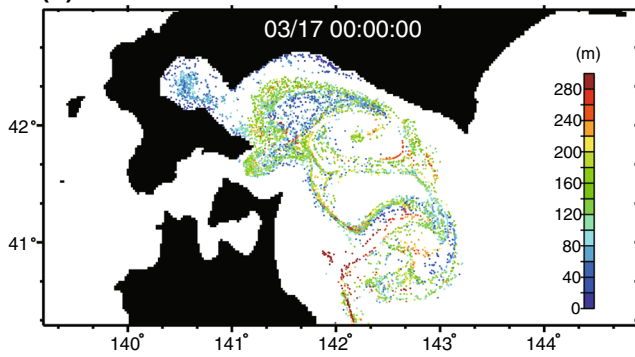
(b) 20-day Integration



(c) 30-day Integration

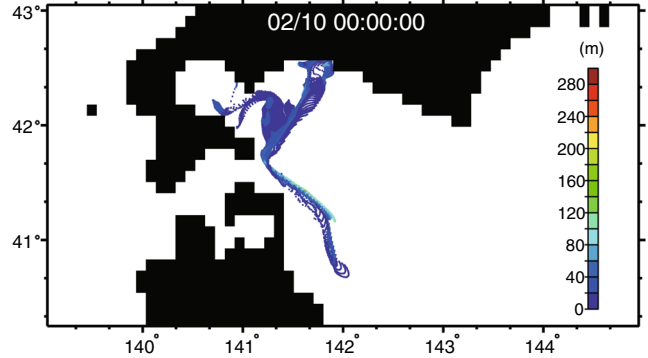


(d) 45-day Integration

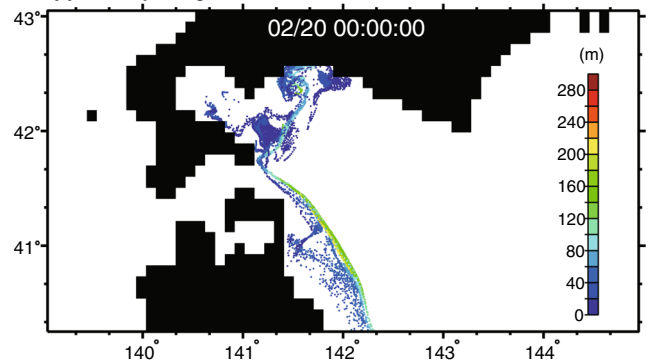


Case L0

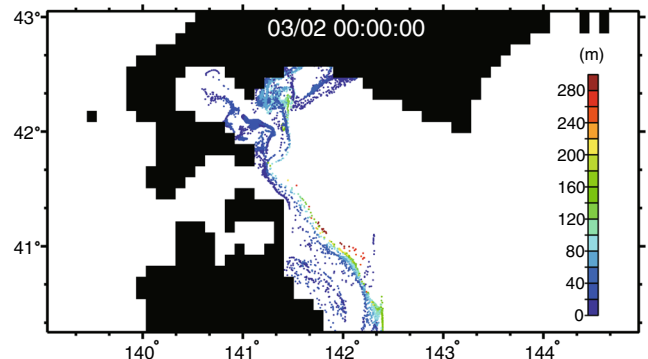
(e) 10-day Integration



(f) 20-day Integration



(g) 30-day Integration



(h) 45-day Integration

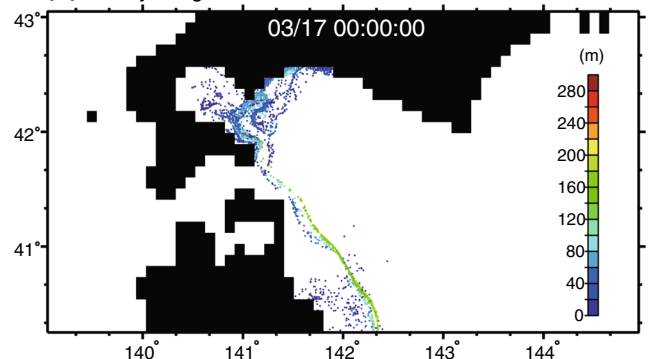


Fig. 6 Distribution of particles under the passive transport condition after (a, e) 10 days, (b, f) 20 days, (c, g) 30 days, and (d, h) 45 days of integration. *Left and right panels* denote PT experiments based on the 1/50° and 1/10° models (cases H0 and L0), respectively. Particle color indicates the vertical position

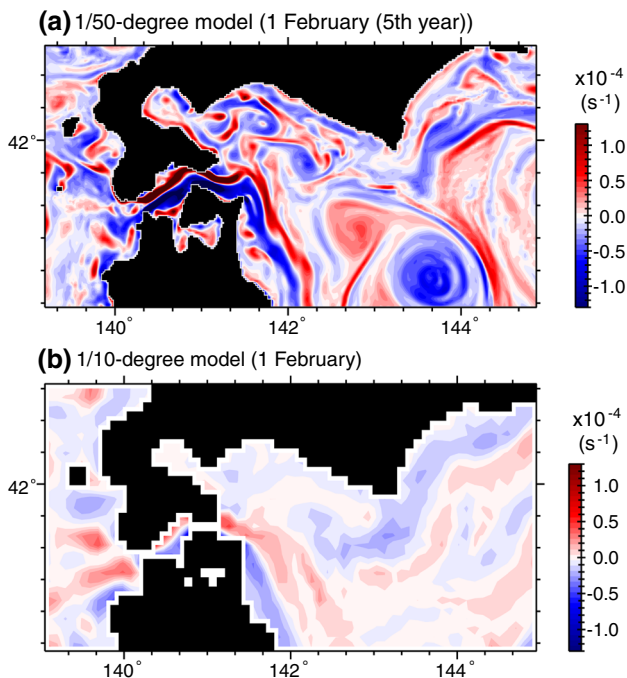


Fig. 7 Daily mean relative vorticities at the sea surface on 1 February for the a 1/50° and b 1/10° models

characterized mainly by anticlockwise circulation (10–20 cm/s) on the slope and southeastward flows (5–15 cm/s) along the coast parallel to the northwest–southeast direction (i.e., the dominant wind-stress direction), as reported in previous studies [12]. A new finding from the present simulation is that there is a branch of the CO that is separated from the northern part of the anticlockwise circulation. Part of the northern branch also seems to flow into the central part of the bay mouth and then join the southeastward wind-driven current near the coast.

Vertical sections of the average northwestward velocities and salinities in February at the mouth of Funka Bay (thick line in Fig. 4) indicate an inflow-outflow structure (Fig. 5). The low-salinity water corresponding to the CO water flows into the bay through the northern and central parts of the bay mouth at speeds of 0–5 cm/s, whereas the high-salinity water corresponding to the Fw water flows out through the southern part at speeds of 0 to –15 cm/s. The outflow intensifies near the bottom. This inflow-outflow structure is also expected to contribute to the transport of the eggs and larvae into/out of the bay, which is examined in the next section.

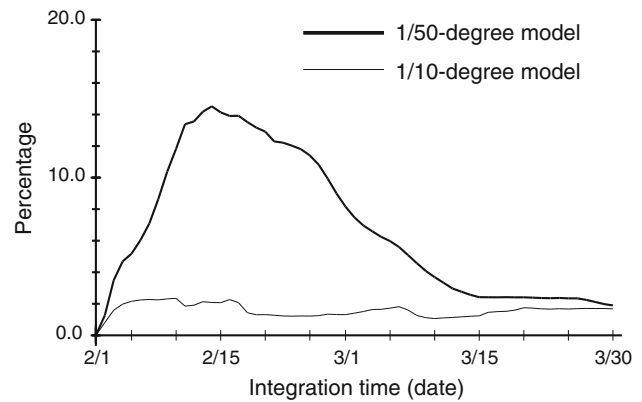


Fig. 8 Time series of the residual ratio, as estimated by dividing the number of particles present in Funka Bay by the number of particles released. *Thick and thin lines* represent the ratios for the 1/50° and 1/10° models (cases H0 and L0), respectively

Particle tracking experiments

The tracked particles were initially set at a depth of 10 m in the gray region near Funka Bay (Fig. 1). Results of the PT experiment based on the 5-year simulation are shown here as representative results. First, the spatiotemporal distribution of particles transported under the passive transport condition (Eq. 1) are compared between the 1/50° (case H0) and the 1/10° (case L0) models (Fig. 6). The vertical positions of the particles are indicated by the particular color used. Even though the same sea surface forcings were applied, there are clearly many differences between the results of the two models. We now focus on three particular differences between them.

The first difference is that there is a much higher horizontal dispersion of particles for the 1/50° model (Fig. 6). Daily mean values of relative vorticity at the sea surface on 1 February are shown for the two models in Fig. 7. The magnitude of the relative vorticity is larger and the positive–negative contrast in relative vorticity is greater for the 1/50° model. This indicates that small-scale submesoscale variations with typical spatial scales of 10–20 km are enhanced in the 1/50° model, which induces greater particle dispersion.

The second difference is in the behavior of particles that are transported into/out of Funka Bay. This behavior is monitored via the residual ratio, which is estimated by dividing the number of particles present within the bay by the total number of particles released (Fig. 8). The residual ratio is fairly similar in the two models at the end of the PT experiments, but the transport process for the particles clearly differs between the models: particles are quite easily transported into/out of Funka Bay in the 1/50° model, in contrast to what is seen in the 1/10° model. Although the transport pathway of each particle cannot be discerned from Fig. 6a–d, it was found (although it is not shown here) that

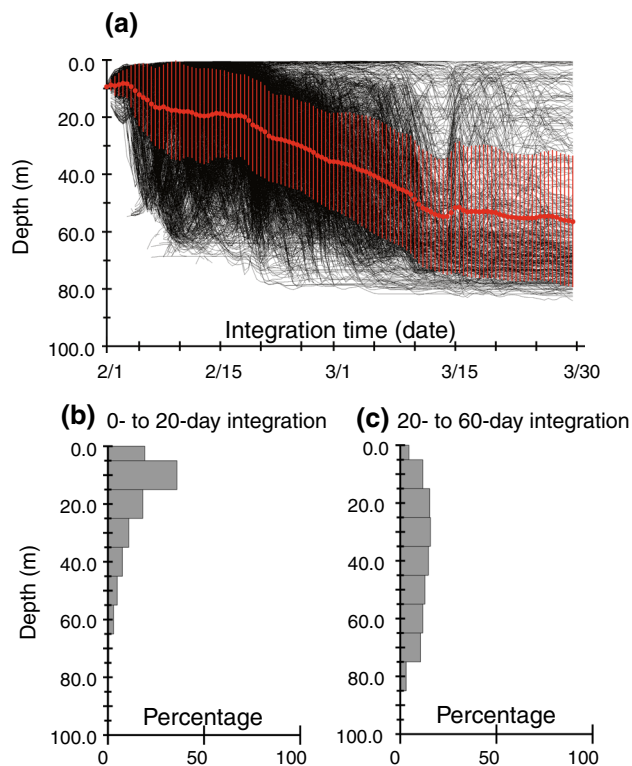


Fig. 9 Vertical positions of the particles in Funka Bay. **a** Vertical trajectories of all of the particles in Funka Bay are illustrated by thin black lines. Mean and standard deviation are denoted by a red closed circle and a vertical bar, respectively. The frequency distributions of the particles in Funka Bay during **b** days 0–20 and **c** days 20–60 correspond roughly to the egg and larval stages, respectively

most of the particles in the $1/50^\circ$ model are transported into the bay from the northern part of the mouth of the bay in an anticlockwise manner along the coast, and out of the southern part of the mouth of the bay, as inferred from the mean velocities in February (Figs. 4, 5).

The third difference is in the vertical positions of the particles. Drastic vertical movements can be seen in the $1/50^\circ$ model (Fig. 6a–d). Some of the particles sink to depths of >200 m. This can be attributed to submesoscale variations enhancing the downward velocities in the $1/50^\circ$ model (not shown). However, eggs and larvae of the Japanese Pacific walleye pollock have not actually been observed at such a deep subsurface [25, 46].

Focusing on the vertical positions of the particles in Funka Bay, we found that particles tend to sink gradually over time to the subsurface (Fig. 9a). When the PT period is separated into days 0–20 and days 20–60, which correspond roughly to the egg and larval stages, respectively, the vertical positions of the particles tend to be nearly homogeneous for the latter (Fig. 9c). In contrast, previous studies [25, 46] have reported that most of the eggs and larvae near Funka Bay are distributed at depths of <40 m

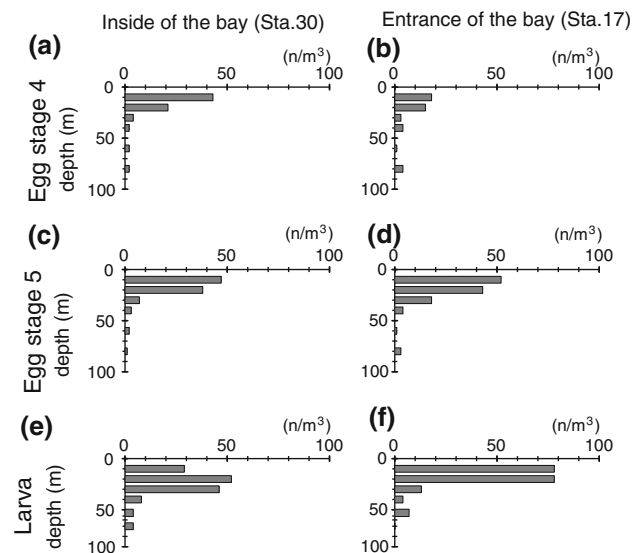


Fig. 10 Vertical distributions of stage 4 eggs (upper: **a**, **b**), stage 5 eggs (middle: **c**, **d**), and larvae (lower: **e**, **f**) of walleye pollock in Funka Bay on March 15–16, 1982. Collections were performed with MTD nets at 6 layers (10, 20, 30, 40, 60, and 80 m) [25]. The vertical distributions inside (left: **a**, **c**, **e**) and at the entrance to (right: **b**, **d**, **f**) the bay are shown

(Fig. 10). This indicates that the vertical movements of the particles cannot be accurately explained by the passive transport condition; that is, there must be a non-passive effect that keeps the eggs and larvae near the sea surface.

Additional PT experiments were performed under the non-passive transport condition governed by Eqs. 2, 3, including buoyancy velocity and turbulent diffusion. The vertical distributions of the particles in Funka Bay seen in cases H1–H5 (Fig. 11) clearly differ from that seen in case H0 (Fig. 9). The particle positions in cases H1–H4 are limited to depths of 0–40 m. Similar behavior is observed even when the vertical turbulence is removed from Eq. 2 (not shown). This indicates that buoyancy is needed to keep the eggs and larvae near the sea surface. The particle densities for cases H1–H4 are always less than the density of the water in the winter mixed layer around Funka Bay (1026 – 1026.5 kg/m^3).

Slight differences can be seen in the vertical positions of particles between cases H1–H3 and case H4, but not case H5 (Fig. 11). For instance, the vertical distribution in case H4 tends to exhibit a weak local maximum in the subsurface after 20 days (Fig. 11i), which roughly corresponds to the larval stage. A similar subsurface maximum is found for the observed distribution of larvae in Funka Bay (Fig. 10e), although the observed maximum appears at a depth of 20 m, which is deeper than that for case H4 by 10 m. It is worth recalling that the particle density in case H4 is not in the range of egg densities that were measured in a laboratory experiment (1020 – 1025 kg/m^3) [27], and

Fig. 11 Same as Fig. 9b, c (case H0), but for cases H1–H5. **a–e** H1–H5, respectively, for days 0–20. **f–j** H1–H5, respectively, for days 20–60

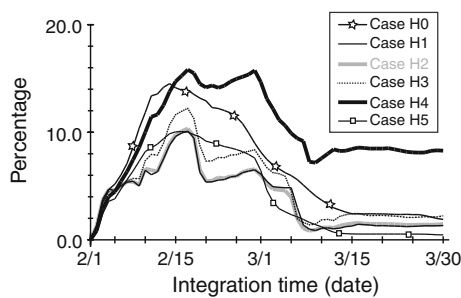
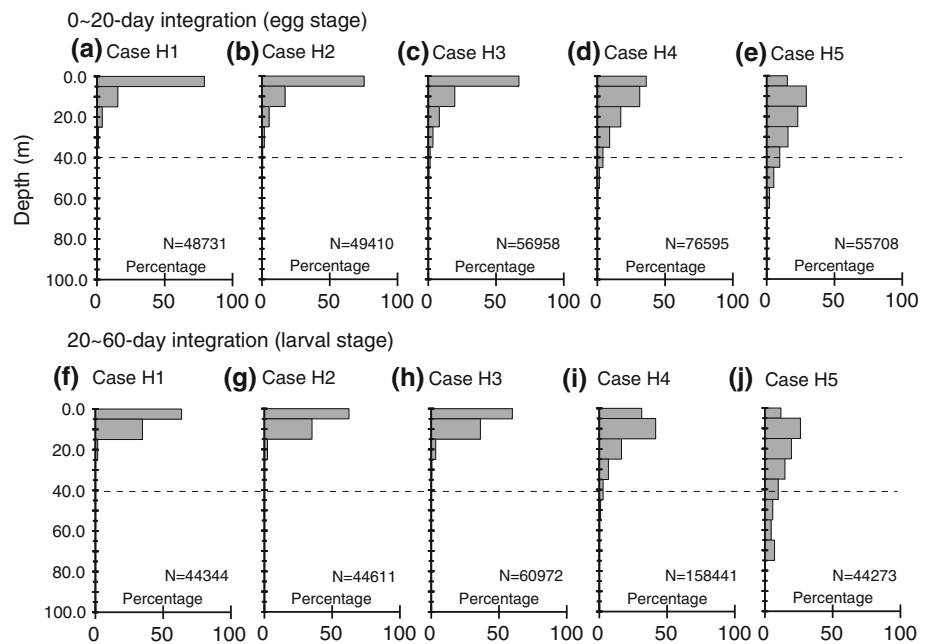


Fig. 12 Same as Fig. 8 (case H0), but for cases H0–H5

the particle diameter is fixed. These imply that, among all of the cases, case H4 yields a vertical distribution of particles that is the closest to the profile observed in all of the PT experiments, although the equations governing vertical motion are not completely accurate. Aspects of the present study that should be modified in future work are discussed in the next section.

Moreover, it should be emphasized that, regardless of the slight difference in vertical positions between cases H1–H3 and case H4 (Fig. 11), there is a great difference between them in terms of the residual ratio of particles (Fig. 12). The residual ratio of particles is the highest for case H4, indicating that the residual ratio within Funka Bay is rather sensitive to the vertical motions/positions of the eggs and larvae.

Discussion

We now discuss the possible reasons that case H4 has the highest residual ratio. Case H4 had the highest residual

ratio even when the initial time of the PT experiment was changed from 1 January to 1 March in years 2–5 (not shown) instead of 1 February in year 5 (Figs. 11, 12). The fact that case H4 had the highest residual ratio, even for different PT periods, can be interpreted as follows.

The number of particles transported into/out of the bay was counted at 12-h intervals in cases H4 and H1 (here, we have selected H1 as an example from among cases H1–H3). The number of all inflowing/outflowing particles and the number of particles that remained in the bay until the end of the PT experiment (“remaining particles”) were counted separately. The variation in the number of inflowing particles over time before the 20-day integration appears to be similar in both cases (Fig. 13); a large number of particles are transported into the bay. The inflow of particles decreases drastically after 20 days in case H1 (Fig. 13a), whereas the inflow of particles continues after 20 days in case H4 (Fig. 13b). The particles that flow in after 20 days (thick line in Fig. 13b) tend to be consistent with the remaining particles (the thin line in Fig. 13b). This implies that particles distributed outside of the bay at 20 days contribute significantly to the highest residual ratio exhibited by case H4.

The horizontal distributions of the remaining particles at 0 (red circles) and 20 (blue circles) days are shown in Fig. 14. There is a high concentration of particles near the coast east of Funka Bay at day 20 in case H4 (blue circles in Fig. 14b), and this is the primary source of the remaining particles (Fig. 13). In the typical transport process into the bay after 20 days (not shown), particles distributed outside of the bay are transported in an anticlockwise manner along the coast and into the bay from the northern part of the bay

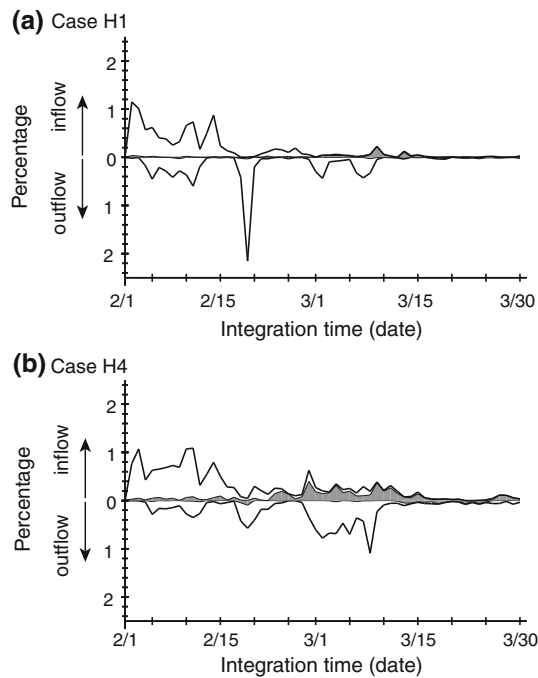


Fig. 13 Number of particles transported into and out of Funka Bay in cases H1 (**a**: upper panel) and H4 (**b**: lower panel), counted at 12-h intervals. They are also counted separately according to whether or not the particles remain within the bay until the end of the PT experiment (i.e., 31 March). A *thick line* (*thin line with a gray area*) corresponds to all inflowing/outflowing particles (the particles that remain in the bay until the end). The number of particles is divided by the number of particles released, as well as Figs. 8 and 12

mouth (Fig. 5), accompanied by the nearshore part of the CO (Figs. 3, 4). In contrast, this high-concentration area barely forms in case H1 (blue circles in Fig. 14a); instead, most of the particles are widely dispersed, so stagnation does not occur near the coast. As a result, the vertical positions/motions of particles that avoid the top of the sea surface in case H4 (Fig. 11i) lead to the stagnation of particles near the coast east of the bay. The dynamics with respect to the stagnation in the subsurface is an important issue, though it is beyond the scope of this article.

The important point here is that the above transport process for particles into Funka Bay is inconsistent with the transport process derived from PT experiments based on the barotropic model [14], in which the eggs are transported into the bay by the wind-driven vortex pair while the CO prevents the eggs from flowing into the bay. Originally, the barotropic model computed two-dimensional velocities averaged from the sea surface to the bottom, meaning that the PT experiment based on the barotropic model is valid for areas where vertically homogeneous flows are dominant. However, it is difficult to justify an assumption that the current structure around Funka Bay is a homogeneous flow (Fig. 5). Moreover, it is not possible to deal with the inhomogeneous vertical

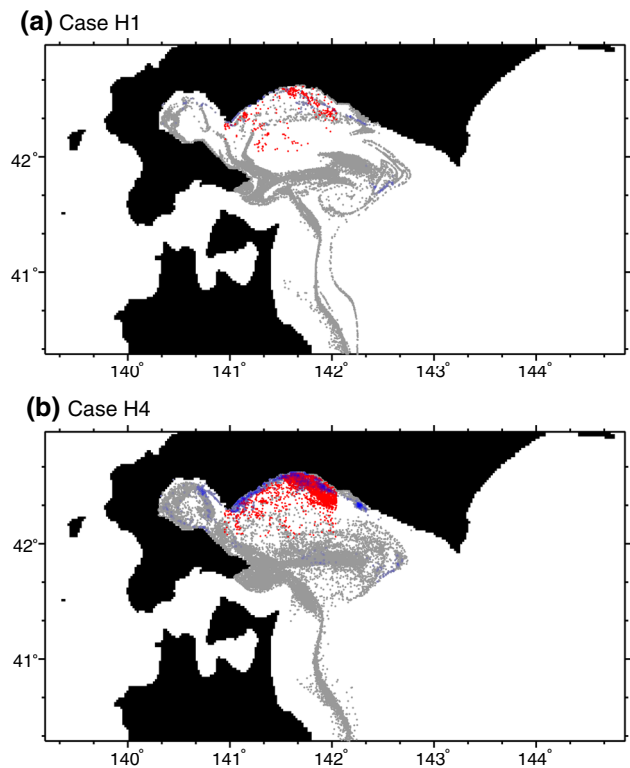


Fig. 14 Distributions of the particles that remained in Funka Bay until the end of the PT experiments at 0 (*red circle*) and 20 days (*blue circles*) for cases H1 (**a**: upper panels) and H4 (**b**: lower panel). *Gray closed circles* denote the distribution of other particles at 20 days

distribution of particles (Figs. 10, 11) in the PT experiment based on the barotropic model.

It should be re-emphasized that, for the first time, the results of the present study highlight the important effect of the vertical motions/positions of the particles on the residual ratio of the eggs and larvae within Funka Bay, which is expected to be linked to recruitment. However, the settings of the PT experiment in this study must be modified in the following manner to elucidate the year-to-year variations in the transport process of the eggs and larvae. (1) The high-resolution ocean model should be updated to reproduce the year-to-year oceanographic conditions around Funka Bay. (2) The initial positions of the particles, which potentially change from year to year, should be determined on the basis of observations or statistical estimation [24]. (3) The vertical motions of the particles should be formulated more appropriately. Two formulation methods could probably be applied in future work. One is to introduce complicated biological processes into the vertical motions of the particles; the other is to statistically simplify the vertical distributions of the particles. To implement the former method, it is necessary to obtain biological parameters such as temporal changes in the density, size, and shape of the eggs and larvae as well as

the vertical swimming ability and temperature selectivity of the larvae in laboratory experiments (Sakurai and Yamamoto, pers. comm., 2013). To apply the latter method, additional oceanographic and biological field data are required so that a robust statistical formulation can be constructed. In particular, much more data on the vertical distribution of the larvae must be collected, because current data on this distribution are limited and were recorded more than 30 years ago (e.g., Fig. 10).

Finally, we again mention that our ultimate goal is to develop an IBM of Japanese Pacific walleye pollock by systematically integrating oceanographic and biological studies. This can then be applied in stock assessment and recruitment prediction. Stock assessment [2] is primarily based on a statistical VPA method, which has given us valuable information. However, the VPA-based method potentially includes uncertainties and assumptions, just like the IBM-based method. Hence, it may be preferable to combine results from the VPA- and IBM-based methods in a complementary manner to gain a deeper understanding of the year-to-year dynamics of the stock/recruitment and to enhance assessment accuracy.

Acknowledgments We would like to deeply thank Dr. Makino for providing us with the valuable opportunity to produce this manuscript. We also would like to thank the editor, two anonymous reviewers, and Dr. Isoda (Hokkaido University) for constructive and fruitful comments. Our numerical simulation was conducted on a cluster and vector computing system at the Agriculture, Forest, Fisheries, and Technology Center. This work was supported mainly by the Fisheries Agency project (Shigen HendoYoin Bunseki Chosa), but the contents of this study do not necessarily reflect the views of the Fisheries Agency.

References

- Shida O, Hamatsu T, Nishimura A, Suzaki A, Yamamoto J, Miyashita K, Sakurai Y (2007) Interannual fluctuations in recruitment of walleye pollock in the Oyashio region related to environmental changes. *Deep Sea Res II* 54:2822–2831
- Mori K, Funamoto T (2009) Assessments of fishery stocks in the Japanese Waters. Stock assessment of Japanese Pacific population of walleye pollock in 2008. Fisheries Agency and Fisheries Research Agency of Japan, Tokyo, pp 395–441 (in Japanese)
- Nakatani T, Sugimoto K, Takatsu T, Takahashi T (2003) Environmental factors in Funka Bay, Hokkaido, affecting the year class strength of walleye pollock, *Theragra chalcogramma*. *Bull Jpn Soc Fish Oceanogr* 67:23–28 (in Japanese with English abstract)
- Kendall WA, Schumacher DJ, Kim S (1996) Walleye pollock recruitment in Shelikof Strait: applied fisheries oceanography. *Fish Oceanogr* 5:4–18
- Wespstad GV, Fritz WL, Ingraham JW, Megrey AB (2000) On relationships between cannibalism, climate variability, physical transport, and recruitment success of Bering Sea walleye pollock (*Theragra chalcogramma*). *ICES J Mar Sci* 57:272–278
- Bailey MK, Stabeno JP, Powers AD (1997) The role of larval retention and transport features in mortality and potential gene flow of walleye pollock. *J Fish Biol* 51:135–154
- Yoon TH (1981) Reproductive cycle of female walleye pollock, *Theragra chalcogramma* (Pallas), in the adjacent waters of Funka Bay, Hokkaido. *Bull Fac Fish Hokkaido Univ* 32:22–38 (in Japanese with English abstract)
- Maeda T (1986) Life cycle and behavior of adult pollock (*Theragra chalcogramma*) (PALLAS) in water adjacent to Funka Bay, Hokkaido Island. *Int North Pac Fish Comm Bull* 45:39–65
- Kendall WA, Nakatani T (1992) Comparisons of early-life-history characteristics of walleye pollock *Theragra chalcogramma* in Shelikof Strait, Gulf of Alaska, and Funka Bay, Hokkaido, Japan. *Fish Bull US* 90:129–138
- Honda S, Oshima T, Nishimura A, Hattori T (2004) Movement of juvenile walleye pollock, *Theragra chalcogramma*, from a spawning ground to a nursery ground along the Pacific coast of Hokkaido Japan. *Fish Oceanogr* 13(Suppl 1):84–98
- Nakatani T, Maeda T (1981) Transport process of Alaska pollock eggs in Funka Bay and the adjacent waters, Hokkaido. *Bull Jpn Soc Fish Oceanogr* 47:1115–1118
- Kuroda H, Isoda Y, Takeoka H, Honda S (2006) Coastal current on the eastern shelf of Hidaka Bay. *J Oceanogr* 62:731–744
- Ohtani K, Akiba Y, Yoshida K, Ohtsuki T (1971) Studies on the change of the hydrographic conditions in the Funka Bay III. Oceanic conditions of the Funka Bay occupied by the Oyashio waters (in Japanese with English abstract). *Bull Fac Fish Hokkaido Univ* 22:129–142
- Shimizu M, Isoda Y (1998) Numerical simulations of the transport process of walleye pollock eggs into Funka Bay. *Mem Fac Fish Hokkaido Univ* 45:56–59
- Sakamoto K, Tsujino H, Nishikawa S, Nakano H, Motoi T (2010) Dynamics of the coastal Oyashio and its seasonal variation in a high-resolution western North Pacific ocean model. *J Phys Oceanogr* 40:1283–1301
- Shchepetkin AF, McWilliams JC (2003) A method for computing horizontal pressure-gradient force in an oceanic model with a nonaligned vertical coordinate. *J Geophys Res* 108(C3):3090. doi:10.1029/2001JC001047
- Shchepetkin AF, McWilliams JC (2005) The Regional Ocean Modeling System (ROMS): a split explicit, free-surface, topography-following-coordinate oceanic model. *Ocean Model* 9:347–404
- Guo X, Fukuda H, Miyazawa Y, Yamagata T (2003) A triply nested ocean model for simulating the Kuroshio—roles of horizontal resolution on JEBAR. *J Phys Oceanogr* 33:146–169
- Penven P, Debreu L, Marchesiello P, McWilliams JC (2006) Evaluation and application of the ROMS 1-way embedding procedure to the central California upwelling system. *Ocean Model* 12:158–187
- Kuroda H, Setou T, Aoki K, Takahashi D, Shimizu M, Watanabe T (2013) A numerical study of the Kuroshio-induced circulation in Tosa Bay, off the southern coast of Japan. *Cont Shelf Res* 53:50–62
- Large W, Yeager S (2004) Diurnal to decadal global forcing for ocean and sea-ice models: the data sets and flux climatologies. NCAR Tech Note NCAR/TN-460+STR. National Center for Atmospheric Research, Boulder
- Nakatani T, Maeda T (1989) Distribution of copepod nauplii during the early life stage of walleye pollock in Funka Bay and vicinity, Hokkaido. In: Proceedings of International Symposium on Biology and Management of Walleye Pollock. AK-SG-89. University of Alaska, Fairbanks, pp 217–240
- Nakatani T, Sugimoto K (1998) 13. Survival of walleye pollock in early life stages in Funka Bay and the surrounding vicinity in Hokkaido. *Mem Fac Fish Hokkaido Univ* 45:64–70

24. Yabe I, Kusaka A, Hamatsu T, Azumaya T, Nishimura A (2011) Water mass structure in the spawning area of walleye pollock (*Theragra chalcogramma*) on the Pacific coast of the southern Hokkaido, Japan. *Bull Jpn Soc Fish Oceanogr* 75:211–220
25. Nakatani T (1988) Studies on the early life history of walleye pollock *Theragra chalcogramma* in Funka Bay and vicinity, Hokkaido. *Mem Fac Fish Hokkaido Univ* 35:1–46
26. Maeda T, Takahashi T, Ijichi M, Hirakawa H, Ueno M (1976) Ecological studies on the Alaska pollock in the adjacent waters of the Funka Bay, Hokkaido. II. Spawning season. *Nippon Suisan Gakkaishi* 42:1213–1222 (in Japanese with English abstract)
27. Yamamoto J, Osato M, Sakurai Y (2009) Does the extent of ice cover affect the fate of walleye pollock? *PICES Sci Rep* 36:289–290
28. Nishimura A, Hamatsu T, Shida O, Mihara I, Mutoh T (2007) Interannual variability in hatching period and early growth of juvenile walleye pollock, *Theragra chalcogramma*, in the Pacific coastal area of Hokkaido. *Fish Oceanogr* 16:229–239
29. Nakatani T, Maeda T (1984) Thermal effect on the development of walleye pollock eggs and their upward speed to the surface. *Nippon Suisan Gakkaishi* 50:937–942 (in Japanese with English abstract)
30. Visser WA (1997) Using random walk models to simulate the vertical distribution of particles in a turbulent water column. *Mar Ecol Prog Ser* 158:275–281
31. Itoh M, Ohshima IK (2000) Seasonal variations of water masses and sea level in the southwestern part of the Okhotsk Sea. *J Oceanogr* 56:643–654
32. Simizu D, Ohshima KI (2002) Barotropic response of the Sea of Okhotsk to wind forcing. *J Oceanogr* 58:851–860
33. Mizuta G, Fukamachi Y, Ohshima KI, Wakatsuchi M (2003) Structure and seasonal variability of the East Sakhalin Current. *J Phys Oceanogr* 33:2430–2445
34. Fukamachi Y, Mizuta G, Ohshima KI, Talley LD, Riser SC, Wakatsuchi M (2004) Transport and modification processes of dense shelf water revealed by long-term mooring off Sakhalin in the Sea of Okhotsk. *J Geophys Res* 109:C09S10. doi:10.1029/2003JC001906
35. Simizu D, Ohshima KI (2006) A model simulation on the circulation in the Sea of Okhotsk and the East Sakhalin Current. *J Geophys Res* 111:C05016. doi:10.1029/2005JC00298
36. Ebuchi N (2006) Seasonal and interannual variations in the East Sakhalin Current revealed by TOPEX/POSEIDON altimeter data. *J Oceanogr* 62:171–183
37. Ebuchi N, Fukamachi Y, Ohshima KI, Shirasawa K, Ishikawa M, Takatsuka T, Daibo T, Walatsuchi M (2006) Observation of the Soya Warm Current using HF ocean radar. *J Oceanogr* 62:47–61
38. Isoda Y, Kuroda H, Myousyo T, Honda S (2003) Hydrographic feature of coastal Oyashio and its seasonal variation. *Bull Coast Oceanogr* 41:5–12 (in Japanese with English abstract)
39. Kusaka A, Ono T, Azumaya T, Kasai H, Oguma S, Kawasaki Y, Hirakawa K (2009) Seasonal variations of oceanographic conditions in the continental shelf area off the eastern Pacific coast of Hokkaido, Japan. *Oceanogr Jpn* 18:135–156 (in Japanese with English abstract)
40. Rosa AL, Isoda Y, Uehara K, Aiki T (2007) Seasonal variations of water system distribution and flow patterns in the southern sea area of Hokkaido, Japan. *J Oceanogr* 63:573–588
41. Ogasawara J (1987) The Oyashio and the Oyashio Littoral Current. *Kaiyo Monthly* 19:21–25 (in Japanese)
42. Shimizu M, Isoda Y, Baba K (2001) A late winter hydrography in Hidaka Bay, south of Hokkaido, Japan. *J Oceanogr* 57:385–395
43. Conlon DM (1980) On the outflow modes of the Tsugaru Warm Current. *La Mer* 20:60–64
44. Ohtani K (1971) Studies on the change of the hydrographic conditions in the Funka Bay II. Characteristics of the waters occupying the Funka Bay. *Bull Fac Fish Hokkaido Univ* 22:58–66 (in Japanese with English abstract)
45. Miyake H, Tanaka I, Murakami T (1988) Outflow of water from Funka Bay, Hokkaido, during early spring. *J Oceanogr Soc Jpn* 44:163–170
46. Kendall AW (2001) Specific gravity and vertical distribution of walleye pollock (*Theragra chalcogramma*) eggs. *Alaska Fish Sci Cent Process Rep* 2001–01:88p